

ICON E-8542

A FINITE ELEMENT MODEL FOR PRE- AND POSTTEST CALCULATIONS OF THE FOREVER-EXPERIMENTS

H.-G. Willschuetz
Forschungszentrum Rossendorf e. V.
Institute of Safety Research
P. O. Box 51 01 19
D - 01314 Dresden
Germany
Phone ++49 351 260 3431
Fax ++ 49 351 260 2002
H.G.Willschuetz@fz-rossendorf.de

E. Altstadt
Forschungszentrum Rossendorf e. V.
Institute of Safety Research
P. O. Box 51 01 19
D - 01314 Dresden
Germany
Phone ++49 351 260 2776
Fax ++ 49 351 260 2002
E.Altstadt@fz-rossendorf.de

F.-P. Weiss
Forschungszentrum Rossendorf e. V.
Institute of Safety Research
P. O. Box 51 01 19
D - 01314 Dresden
Germany
Phone ++49 351 260 3480
Fax ++ 49 351 260 3440
F.P.Weiss@fz-rossendorf.de

B. R. Sehgal
Royal Institute of Technology
Division of Nuclear Power Safety
Drottning Kristinas väg 33A
S - 10044 Stockholm
Sweden
Phone ++46 8 790 9252
Fax ++46 8 790 9197
sehgal@ne.kth.se

KEYWORDS: FINITE ELEMENT CALCULATIONS, FOREVER-EXPERIMENT, COUPLING OF THERMO-FLUID DYNAMIC
AND STRUCTURAL MECHANICAL MODEL, ADVANCED CREEP MODELLING

ABSTRACT

To get an improved understanding of the processes occurring during the late phase of a core melt down accident the FOREVER-experiments are currently underway.

These experiments are simulating the behaviour of the RPV lower head under the thermal loads of a convecting melt pool with decay heating and simultaneous pressure loads. The geometrical scale of the experiments is 1:10 compared to a common Light Water Reactor.

Due to the multi axial creep deformation of the vessel with a non-uniform temperature field these experiments are on the one hand an excellent source of data to validate creep models for different pressure vessel steels; and on the other hand the results of pre-test calculations can be used to optimize the experimental procedure.

In this paper a Finite Element model is developed:

- using the Computational Fluid Dynamics module the temperature field within the melt pool and within the vessel wall is evaluated.

- transient structural mechanical calculations are then performed applying an advanced creep model which takes into account large temperature, stress and strain variations.

Post test calculations of the FOREVER-C2 experiment were performed. If the temperature field in the vessel wall is fixed along creeping process, the calculated creep curves disagree with the measurement. Considering the variation of the temperature field, the calculated results show a good agreement with the measurements.

INTRODUCTION

For future nuclear power plants it is demanded that there are no consequences for the environment and the population even in the closest vicinity of the plant during, and after, any conceivable accident scenario. This includes the hypothetical scenario of a severe accident with subsequent core meltdown and formation of a melt pool in the lower plenum of the reactor pressure vessel (RPV) of a Light Water Reactor (LWR). One accident management strategy is to stabilize the in-vessel debris configuration in the RPV and use that as the major barrier against uncontrolled release of heat and radio nuclides. This strategy also applies to existing plants.

To obtain an improved understanding and knowledge of the melt pool convection and the timing and mode of the vessel creep failure during the late phase of a core melt down accident the FOREVER-experiments (Failure Of REactor Vessel Retention) are currently underway at the Division of Nuclear Power Safety of the Royal Institute of Technology Stockholm (Sehgal et al., 1999).

These experiments are simulating the behaviour of the lower head of the RPV under the thermal loads of a convecting melt pool with decay heating, and under the pressure loads that the vessel may experience in a depressurization scenario. The geometrical scale of the experiments is 1:10 compared to a common Light Water Reactor (LWR).

The FOREVER program consists of three major phases. During the first series of experiments the creep behaviour and failure (FOREVER-C) of the vessel under the attack of the melt pool and an internal pressure load is investigated. It is intended to maintain the creep process until vessel failure.

Due to the multi axial creep deformation of the vessel with a non-uniform temperature field these experiments are on the one hand an excellent source of data to validate creep models for pressure vessel steels which are developed on the basis of uniaxial creep tests. On the other hand the results of pre-test calculations can be used to optimize the experimental procedure with considerations of the uncertainties in the applied models and assumed boundary conditions.

Therefore, a two-dimensional Finite Element (FE) model is developed, based on the multi-purpose code ANSYS/Multiphysics® at the Institute of Safety Research at the Forschungszentrum Rossendorf, Dresden, Germany. Using the Computational Fluid Dynamics (CFD) module the temperature field within the melt pool and within the vessel wall is evaluated. The transient structural mechanical calculations are, then, performed applying a creep model which takes into account large temperature, stress and strain variations.

This numerical approach avoids the use of a single creep law (e.g. strain hardening model) with parameters evaluated from a limited stress and temperature range. Instead of this strain rate - strain relations can be applied which are separately fitted for different temperature and stress levels.

Performing post-test calculations for the FOREVER-C2 experiment it was found that the comparison of the experimental data with the predicted numerical results has to be done carefully. On the one hand measured data on melt pool temperature was quite meager during the late phase of the experiment when many thermocouples, at high temperature locations, failed. On the other

hand the calculated results for the creep process show great sensitivity to small changes in the temperature and structure-mechanical boundary conditions. For example in the experiment an increasing creep strain rate was observed. The numerical simulation shows that this accelerated creep could be due to a slight temperature increase rather than to the tertiary creep phase.

Taking into account both - experimental and numerical results - provides a good opportunity to improve the simulation and the understanding of the vessel failure mechanisms. Of particular interest are (i) the time to failure and (ii) the location and mode of failure.

NOMENCLATURE

Latin

a	thermal diffusivity	[m ² /s]
C	model constant	[-]
D	damage parameter	[-]
e	emissivity	[-]
g	gravitational acceleration	[m/s ²]
k	turbulent kinetic energy	[m ² /s ²]
P	pressure	[Pa]; [bar]
q	volumetric heat generation	[W/m ³]
Q	total heat generation	[W]; [VA]
r	radius	[m]
Ra	Rayleigh-number	[-]
s	wall thickness	[m]
t	time	[s]
T	temperature	[°C]; [K]
u,v,w	velocities	[m/s]
U	displacement	[m]
W	weighting factor	[-]
x	horizontal (radial) coordinate	[m]
y	vertical (axial) coordinate	[m]
z	coordinate	[m]

Greek

β	coefficient of thermal expansion	[1/K]
ε	strain	[-]
ε	turbulent kinetic energy dissipation rate	[m ² /s ³]
Θ	azimuthal angle	[°]
λ	heat conductivity	[W/mK]
μ	dynamic viscosity	[kg/ms]
ν	kinematic viscosity	[m ² /s]
ρ	density	[kg/m ³]
σ	stress	[Pa]
σ	model constant	[-]
Φ	viscous dissipation	[W/m ³]

Indices

cr	creep
eqv	equivalent
H	high
i	inner, internal
L	low

max	maximal
min	minimal
s	solidus
steel	steel
sum	summation, total
t	turbulent
frac	fracture, rupture
V	volumetric

ABBREVIATIONS

C	Creep
CFD	Computational Fluid Dynamic
FE	Finite Element
FEM	Finite Element Method
FOREVER	Failure Of REactor VESsel Retention
LDT	Linear Displacement Transducer
LWR	Light Water Reactor
RPV	Reactor Pressure Vessel
TC	ThermoCouple
UPF	User Programmable Feature

EXPERIMENTAL SETUP AND FIRST RESULTS

In Figure 1 the principal setup of the FOREVER C-experiments is shown (Sehgal et al., 1999). Due to the limitation of the heating power ($Q_{\max}=22\text{kW}$) in the C1-experiment the temperature at the outer vessel surface was below 800°C at the beginning of the pressurization phase and decreasing during the creep deformation stage. Therefore the creep strain was limited. In the experiment C2 much higher creep strains were reached due to increased power input ($Q_{\max}>40\text{kW}$) and external temperatures of close to 1000°C were observed in the hot focus region at the upper hemispherical part. The analysis presented in this work is based on the latter experiment.

The hemispherical and the cylindrical part of the vessel have, in principal, inner radii of $r_i=188\text{mm}$. The wall-thickness of the cylindrical part which was made of the German RPV steel 15Mo3 was $s=16.0\text{mm}$. The hemisphere had a designed wall thickness of $s=15.0\text{mm}$ and was made of the French RPV steel 16MND5. Due to the hot-pressing manufacturing of the hemisphere from a plate the wall thickness varied in azimuthal and circumferential direction. A second point to be kept in mind is that the melt was prepared outside the vessel and poured through an internal funnel to one side of the vessel (cf. Fig. 1). It can be assumed that these two factors caused some 3D-bending process resulting in a horizontal movement before and during the creep process of the bottom center of the hemisphere which should only relocate in vertical direction presuming ideal symmetry conditions.

The oxidic melt employed as a simulant for the prototypic $\text{UO}_2\text{-ZrO}_2\text{-Zr}$ melt was a $\text{CaO-B}_2\text{O}_3$ mixture (30-70 wt.-%) which has a solidus temperature of $T_s=1250\text{K}$ and is a rather aggressive oxide, especially at high temperatures. To model the internal decay heat generation specially designed heater rods fixed to an internal insulation-reflector-lid were immersed into the melt from the top. The lid was fixed to the upper part of the vessel. After melt was poured the melt injection orifice in the vessel lid was closed and

the vessel inside could be pressurized by Argon. The FOREVER experiments are performed in a containment.

The total duration of the experiment C2 was nearly 10 hours from the start of pre-heating the vessel to the stop of the data recording at the end of the cooldown and relaxation stage.

Figure 2 shows the time history of the heating power input Q , the internal pressure P and the temperatures at different azimuthal locations of the hemisphere. The angle Θ refers to the global spherical coordinate system located in the center of the hemisphere where $\Theta = 0^{\circ}$ denotes the vertical upward direction, i. e. $\Theta = 180^{\circ}$ denotes the very bottom of the vessel.

Until melt pouring ($t=25\text{-}30\text{min}$) all thermocouples show the same temperature. After some 120 min there was a temporarily heater shut down to install additional cooling units to the power supply cables. With the re-gained power supply and temperature level the system was pressurized at $t=200\text{min}$.

In Figure 3 the total displacement U_{sum} at different positions of the external vessel surface during the course of the experiment is shown. The thermal expansion of the vessel due to the hot melt pool can be seen clearly. The start of the pressurization indicates the beginning of the creep deformation stage. The creep curves show an acceleration of the creep strain which indicates normally tertiary creep, because primary creep curves show a declining strain rate and secondary creep is characterized by a constant creep strain rate. As the names indicate the three creep stages should occur in this sequence. And this behaviour was observed in FOREVER-C1. So far the reason for the observations in C2 is not exactly known.

Due to the creep expansion of the vessel the volume of the hemisphere is increasing to the third power of the increase of the radius. This causes a decreasing melt level and as a consequence in the experiment C2 the uppermost parts of the heater rods were no longer immersed in the pool. Therefore they burned by overheat and the power supply was stopped. Thus, the experiment could not be run until vessel failure. The thermal contraction after heater failure is also visible in Figure 3.

For more detailed description and for scaling considerations of the experimental setup the reader is referred to Sehgal et al. (1999).

THERMO-FLUID-DYNAMIC MODEL AND RESULTS

For the evaluation of the temperature field within the vessel wall the CFD-module FLOTTRAN[®] of the FE-code ANSYS[®] is used. A 2D-axis-symmetric model with appropriate boundary conditions and material properties is developed.

A pure homogenous melt pool is assumed inside the vessel with the surface level set to the welding joint between hemisphere and cylinder. Figure 4 shows the FE-mesh and the thermal boundary conditions. The mesh consist of 1740 elements of which 1400 belong to the liquid region at the beginning of the calculation. Due to some prior estimations it was found that the main heat transfer mechanism at the model boundaries is radiation. Therefore at the vessel outside an radiative heat transfer boundary condition is applied with an ambient temperature of $T_{\text{amb}}=400\text{K}$. During the experiment the external vessel wall was subject to strong oxidization. Owing to the lack of exact steel surface emissivities under these conditions a surface emissivity

of $\epsilon_{\text{steel}}=0.8$ has been used. In fact the emissivity could have been higher, but the chosen value can be considered as appropriate (VDI, 1994; Sala 1984, James and Lord, 1992). Also for the internal surfaces radiative boundary conditions have been modelled: between insulation and melt pool (cf. Fig. 1) T_{amb} was set to 1200K, above insulation it was 800K. The emissivity was the same as on the outside. Of course this is a simple model which has to be improved, but the results show that it works quite satisfactorily for a first attempt.

In the experiment the heat is released at the discrete positions of the heater rods. In the model a homogenous volumetric heat source is assumed which is applied to the volume within which the heaters are to be found. Especially at the very bottom the distance between the heater and the vessel wall has a significant influence on the crust formation, which will be considered later (cf. Fig 4).

The internal Rayleigh number can be employed to assess the idealized configuration:

$$Ra_i = \frac{g\beta q_v r_i^5}{\nu a \lambda} \quad (1)$$

With the applied power range, the melt properties employed and the assumptions made above, the internal Rayleigh number for this configuration is calculated in a range of $Ra_i=0.5 \cdot 10^{10}$ to $Ra_i=1.0 \cdot 10^{10}$. Concerning the modelling approach this Rayleigh number seems to be small enough (Sehgal et al., 1996) to model the heat transfer within the pool by the application of a standard-k-g-turbulence model which is provided by FLOTTRAN®.

The well known equation for the turbulent kinetic energy k in 3D Cartesian coordinates is:

$$\begin{aligned} \frac{\partial \rho k}{\partial t} + \frac{\partial \rho u k}{\partial x} + \frac{\partial \rho v k}{\partial y} + \frac{\partial \rho w k}{\partial z} = \\ \frac{\partial}{\partial x} \left(\frac{\mu_t}{\sigma_k} \frac{\partial k}{\partial x} \right) + \frac{\partial}{\partial y} \left(\frac{\mu_t}{\sigma_k} \frac{\partial k}{\partial y} \right) + \frac{\partial}{\partial z} \left(\frac{\mu_t}{\sigma_k} \frac{\partial k}{\partial z} \right) \\ + \Phi - \rho \epsilon + \frac{C_4 \beta \mu_t}{\sigma_k} g \frac{\partial T}{\partial z} \end{aligned} \quad (2)$$

And the equation for the turbulent dissipation rate g is:

$$\begin{aligned} \frac{\partial \rho \epsilon}{\partial t} + \frac{\partial (\rho u \epsilon)}{\partial x} + \frac{\partial (\rho v \epsilon)}{\partial y} + \frac{\partial (\rho w \epsilon)}{\partial z} = \\ \frac{\partial}{\partial x} \left(\frac{\mu_t}{\sigma_\epsilon} \frac{\partial \epsilon}{\partial x} \right) + \frac{\partial}{\partial y} \left(\frac{\mu_t}{\sigma_\epsilon} \frac{\partial \epsilon}{\partial y} \right) + \frac{\partial}{\partial z} \left(\frac{\mu_t}{\sigma_\epsilon} \frac{\partial \epsilon}{\partial z} \right) \\ + C_{1\epsilon} \frac{\epsilon}{k} \Phi - C_2 \rho \frac{\epsilon^2}{k} + \frac{C_\mu (1 - C_3) \beta \rho k}{\sigma_t} g \frac{\partial T}{\partial z} \end{aligned} \quad (3)$$

where F denotes the viscous dissipation term. The default values of ANSYS® for the model constants ($s_k, s_g, C_{1g}, C_2, C_\mu$) are set according to those proposed by Launder and Spalding (1974). The final term in the equations (2) and (3) is used to model the effect of buoyancy. The default values of C_3 and C_4 are 1.0 and 0.0 respectively, that means there is no contribution due to buoyancy effects in turbulence modelling. To model the unstable stratification at the top in the FOREVER-experiment C_3 was set to 1.0 and C_4 to 0.5.

Assuming slow temperature changes in the vessel wall and in the lower part of the melt pool a dynamic crust is modelled by stopping the solution every 20 seconds and checking the temperature field. For those elements where the melt temperatures are below the solidus temperature of $T_s=1250K$ at all nodes, the material number is changed so that these elements belong to the solid region of the oxidic crust. This approach has been chosen because in future calculations the oxidic crust has to be modelled structurally, too, to be able to model a gap formation between crust and vessel. Figure 5 shows the computational domain with the different materials and the boundary conditions at the surface and at the symmetry line where the free slip condition is applied.

So far different power inputs were modelled in transient calculations starting with homogenous initial temperatures within melt pool and vessel wall. The heat generation rates were chosen according to the experimental range which had changed from 30kW to 45kW (cf. Figs. 2, 3). In these calculations a thermal steady state for the vessel wall was observed after some 20-30min.

In Figure 6 the steady state temperature field for the heat generation case $Q=35kW$ is shown for the whole model. The temperatures range from some 600K at the top of the cylindrical part to nearly 1500K in the upper third of the melt pool. Figure 7 gives a more detailed view of the hemispherical part. For a clearer presentation the temperature scale ranges from 1160K to 1500K, the grey regions of the model have temperatures below 1160K.

The cooling effect at the vessel wall in the melt pool can be recognized easily, also the steep temperature gradient through the upper hemispherical part of the vessel wall caused by the focussed heat transfer in this region. The melt shows a stable stratification in the lower and middle parts of the pool, while it has an unstable behaviour near the pool surface where cold plumes are to be found irregularly except close to the wall. The crust acts as an effective insulation and the vessel temperature drops down towards the bottom center. In Figure 8 the external vessel surface temperature calculated for three different power inputs is compared with the measured temperatures at different times. The positions of the thermocouples (TC) are indicated with squares in the diagram. The connecting lines between the TCs should only give an orientation because the distances between the TCs are too large.

The calculated temperature profiles show good agreement with the measurements in the high temperature region of the vessel (cf. Fig. 8). For the slight offset between the temperature maxima it must be mentioned that the CFD-calculations assume the melt level exactly at the welding joint whereas in reality the melt level could have been 10mm to 20mm higher at the beginning. Later the melt level was decreasing due to the volume expansion of the creeping vessel. Also the vertical movement of the

thermocouples (positions marked with squares in the curves) fixed to the side- and downwards creeping vessel wall is not taken into account in the figure.

The differences near the bottom center could result from the transient increase of the distance between the lowermost parts of the heater to the vessel bottom, which is not modelled so far. Other possibilities are, a lack of the computational model, or the formation of a gap between oxidic crust and vessel, wall which induces additional heat transfer resistance. Examination of the vessel after the experiment can not clearly exclude that there was a gap before heater failure. However, no gap was observed in the examination after the experiment, and no gap is modelled in the computations. Later, it will be seen that the combination of low temperatures and low stresses in this region causes no creep near the bottom centre. Also, the temperatures in the upper part of the cylinder are too low to cause significant damage. Therefore the differences between the calculated values and measurements are acceptable. In future more detailed boundary conditions for the cylinder should improve the results.

So far, no transient CFD-calculation for the whole creep deformation stage has been performed due to the large computational time and data storage requirements. But a full time CFD-calculation for the whole creep deformation stage with detailed time-dependent power input is under preparation and with improved computational resources its results will be available in future.

ADVANCED CREEP MODELLING

In the following sections the model for the structure-mechanical calculations is described. Because of the large spatial and transient temperature and stress changes within the vessel wall a new approach for the numerical creep modelling has been developed.

The creep behaviour of materials is usually described by analytical formulas (creep laws) with a number of free parameters, e.g. the creep strain rate is calculated by:

$$\dot{\epsilon} = c_1 \cdot \sigma^{c_2} \cdot t^{c_3} \cdot \exp\left[-\frac{c_4}{T}\right] \quad (4)$$

The coefficients ($c_1 \dots c_4$ in eq. 4) are obtained by fitting the creep law to creep tests performed at constant load and temperature. However, in practice it is often difficult to achieve a satisfying adjustment for a wide range of temperatures and stresses with only one set of parameters. Instead, it appears that the parameters themselves are functions of the temperature or the stress level. Therefore a supplementary method is developed which allows the creep behaviour of a material to be modelled for different stress and temperature levels independently. This is especially useful if strong stress and/or temperature gradients are present. Additionally it is possible to calculate the creep damage and deactivate elements whose accumulated damage is greater or equal to one.

The user programmable features (UPF) of ANSYS® allow the user to couple his own routines to the standard FE-code. The Digital® Fortran Compiler (Rev. 6.0A) was used for programming and for generating the customized ANSYS-executable on a Windows/NT® platform.

The creep behaviour of a material can be described by the strain hardening representation

$$\dot{\epsilon}^{cr} = f(\epsilon^{cr}; \sigma; T) \quad (5)$$

The time hardening representation, or the work hardening representation, can, in general, be transformed into eq (5). The relation eq (5) is transferred into the ANSYS database by means of a number of discrete pairs of the form

$$\begin{bmatrix} \epsilon_{(1)} & \dot{\epsilon}_{(1)} \\ \vdots & \vdots \\ \epsilon_{(n)} & \dot{\epsilon}_{(n)} \end{bmatrix}_{T=\text{const}; \sigma=\text{const}} \quad (6)$$

Several of such sets for different temperature and stress levels can be combined. The complete creep data base then is shown in table 1.

The first index refers to the temperature, the second index to

T_1			...	T_K		
$\sigma_{1;1}$...	$\sigma_{1;M1}$...	$\sigma_{K;1}$...	$\sigma_{K;MK}$
$\epsilon_{1;1}^{frac}$...	$\epsilon_{1;M1}^{frac}$...	$\epsilon_{K;1}^{frac}$...	$\epsilon_{K;MK}^{frac}$
$N_{1;1}$...	N_{M1}	...	$N_{K;1}$...	$N_{K;MK}$
$(\epsilon_{1;1;1}; \dot{\epsilon}_{1;1;1})$...	$(\epsilon_{1;M1;1}; \dot{\epsilon}_{1;M1;1})$...	$(\epsilon_{K;1;1}; \dot{\epsilon}_{K;1;1})$...	$(\epsilon_{K;MK;1}; \dot{\epsilon}_{K;MK;1})$
\vdots	\ddots	\vdots	\ddots	\vdots	\ddots	\vdots
$(\epsilon_{1;1;N}; \dot{\epsilon}_{1;1;N})$...	$(\epsilon_{1;M1;N}; \dot{\epsilon}_{1;M1;N})$...	$(\epsilon_{K;1;N}; \dot{\epsilon}_{K;1;N})$...	$(\epsilon_{K;MK;N}; \dot{\epsilon}_{K;MK;N})$

Table 1: Principle configuration of a creep database for a temperature range from T_1 to T_K and a stress range from s_1 to s_M including the respective creep rupture strain g^{frac} .

the stress and the third to the strain. K is the number of temperature levels, Mk the number of stress levels within the k-th temperature level and $N_{k;m}$ the number of strain rate-strain pairs for the m-th stress level within the k-th temperature level

The UPF routine user01 (ANSYS, 1998) is used to realize the creep data input into ANSYS. The data must be provided by the user as a set of ASCII files (for each temperature-stress level one file).

To realize the calculation of the creep strain increment according to the non-standard creep law, the UPF usercr.f was modified and linked to the customized ANSYS executable (ANSYS, 1998).

In this routine the scalar creep strain increment $\Delta \epsilon^{cr} = \dot{\epsilon}^{cr} \cdot \Delta t$ is determined from the creep data (cf. Table 1) by multi-linear interpolation:

$$\begin{aligned} \Delta \epsilon^{cr} = & [w_1 \cdot \dot{\epsilon}_{L;L;L} + w_2 \cdot \dot{\epsilon}_{L;L;H} + w_3 \cdot \dot{\epsilon}_{L;H;L} \\ & + w_4 \cdot \dot{\epsilon}_{L;H;H} + w_5 \cdot \dot{\epsilon}_{H;L;L} + w_6 \cdot \dot{\epsilon}_{H;L;H} \\ & + w_7 \cdot \dot{\epsilon}_{H;H;L} + w_8 \cdot \dot{\epsilon}_{H;H;H}] \cdot \Delta t \end{aligned} \quad (7)$$

with w_i being the weighting factors (eq. 8):

$$\begin{aligned} w_1 = & \frac{(T_H - T) \cdot (\sigma_{L;H} - \sigma) \cdot (\epsilon_{L;L;H} - \epsilon)}{(T_H - T_L) \cdot (\sigma_{L;H} - \sigma_{L;L}) \cdot (\epsilon_{L;L;H} - \epsilon_{L;L;L})} \\ w_2 = & \frac{(T_H - T) \cdot (\sigma_{L;H} - \sigma) \cdot (\epsilon - \epsilon_{L;L;L})}{(T_H - T_L) \cdot (\sigma_{L;H} - \sigma_{L;L}) \cdot (\epsilon_{L;L;H} - \epsilon_{L;L;L})} \\ w_3 = & \frac{(T_H - T) \cdot (\sigma - \sigma_{L;L}) \cdot (\epsilon_{L;H;H} - \epsilon)}{(T_H - T_L) \cdot (\sigma_{L;H} - \sigma_{L;L}) \cdot (\epsilon_{L;H;H} - \epsilon_{L;H;L})} \\ w_4 = & \frac{(T_H - T) \cdot (\sigma - \sigma_{L;L}) \cdot (\epsilon - \epsilon_{L;H;L})}{(T_H - T_L) \cdot (\sigma_{L;H} - \sigma_{L;L}) \cdot (\epsilon_{L;H;H} - \epsilon_{L;H;L})} \\ w_5 = & \frac{(T - T_L) \cdot (\sigma_{H;H} - \sigma) \cdot (\epsilon_{H;L;H} - \epsilon)}{(T_H - T_L) \cdot (\sigma_{H;H} - \sigma_{H;L}) \cdot (\epsilon_{H;L;H} - \epsilon_{H;L;L})} \\ w_6 = & \frac{(T - T_L) \cdot (\sigma_{H;H} - \sigma) \cdot (\epsilon - \epsilon_{H;L;L})}{(T_H - T_L) \cdot (\sigma_{H;H} - \sigma_{H;L}) \cdot (\epsilon_{H;L;H} - \epsilon_{H;L;L})} \\ w_7 = & \frac{(T - T_L) \cdot (\sigma - \sigma_{H;L}) \cdot (\epsilon_{H;H;H} - \epsilon)}{(T_H - T_L) \cdot (\sigma_{H;H} - \sigma_{H;L}) \cdot (\epsilon_{H;H;H} - \epsilon_{H;H;L})} \\ w_8 = & \frac{(T - T_L) \cdot (\sigma - \sigma_{H;L}) \cdot (\epsilon - \epsilon_{H;H;L})}{(T_H - T_L) \cdot (\sigma_{H;H} - \sigma_{H;L}) \cdot (\epsilon_{H;H;H} - \epsilon_{H;H;L})} \end{aligned} \quad (8)$$

The quantities without index ϵ, σ, T are the actual values of the current element integration point. The indexed quantities are the values from the creep data base eq. (3). They form the smallest intervals which the actual quantities are enclosed in. The meaning of the indices is L: low bound (largest data base value which is smaller than the actual integration point value) and H: high bound (smallest data base value which is greater than the actual integration point value). The first index refers to the temperature, the second index to the stress and the third to the strain. All stress and strain values used here are equivalent values.

The components of the creep strain tensor increment, $\Delta \epsilon_{kl}^{cr}$, are calculated according to the Prandtl-Reuss flow rule (ANSYS, 1998, Becker, 1995).

The creep data base (cf. Table 1) has to be provided in such a way that the actual temperature and the equivalent stress of the elements do not exceed the maximum values of the creep data base. If the actual temperature or stress values are smaller than the smallest values provided, the creep strain increment is zero for this step.

The material damage due to significant creep strains is modelled by a damage measure which is incrementally accumulated at the end of a load step. The damage increment is:

$$\Delta D = \frac{\Delta \epsilon_{eqv}^{cr}}{\epsilon_{frac}^{cr}(\sigma, T)} \cdot \frac{\sigma_{eqv}}{|\sigma_1 + \sigma_2 + \sigma_3|} \quad (9)$$

with ϵ_{frac}^{cr} being the creep fracture strain of the uniaxial creep test at constant stress and temperature. The factor $\sigma_{eqv} / |\sigma_1 + \sigma_2 + \sigma_3|$ (where σ_{eqv} is the von-Mises equivalent stress) considers the damage behaviour in dependance on the tri-axiality of the stress tensor (Azodi et al., 1996). The damage increment is calculated for each finite element by averaging its nodal equivalent creep strains. The accumulated damage over all load steps is

$$D = \sum_{i=1}^{ldstep} \Delta D_i \quad (10)$$

If the element damage reaches the value of $D=1$, the element is killed by setting its death flag to 1 (refer to the „element birth and death“ section of ANSYS 1998).

The creep fracture strain used for the evaluation of the damage increment can be calculated according to a temperature and stress dependent function with user supplied constants or it is calculated from the creep data base (cf. Table 1) by multi-linear interpolation.

DESCRIPTION OF THE MECHANICAL MODEL

The mechanical 2D-axis-symmetric model representation which approximates the 3D-vessel consists of nearly 340 elements and some 410 nodes with 5 element layers over the wall thickness. A sufficient number of elements over the wall thickness is necessary to model the transient body load of the temperature field which is changing along and perpendicular to the wall surface. This is seen in Figure 9, which shows the temperature field caused by the 30kW-scenario as body load of the mechanical model.

Figure 9 also shows the internal pressure load of $P=2.5\text{MPa}$ and the boundary conditions of zero vertical displacement ($U_y=0$) at the vertical top end and zero radial displacement ($U_x=0$) at the symmetry axis.

For the mechanical calculations isotropic material behaviour is assumed. The temperature dependence of all material properties is considered according to the known values of the French RPV-steel 16MND5 (Sehgal et al., 1999). The creep data base (cf. Table 1) has been generated from the fitted strain curves developed by Ikonen (1999). The stress range of the data base reaches from $\sigma_{\min}=5\text{MPa}$ to $\sigma_{\max}=285\text{MPa}$ and the temperature range goes from $T_{\min}=873\text{K}$ to $T_{\max}=1373\text{K}$. That means the calculation is finished if the corresponding maximum values are exceeded.

Until pressurization of the system the displacement measured by the linear displacement transducers (LDT) is only due to thermal expansion. Therefore the transient creep calculation starts at the pressurization time of $t=12000\text{s}$ (cf. Figs. 3 and 10), in the experiment.

CREEP CALCULATIONS AND FIRST ESTIMATION OF FAILURE TIME

If a constant temperature field is assumed within the vessel wall for the transient creep calculation a typical creep curve will be calculated by the code (see Fig. 10, blue curve). This curve is characterized by a steep - but decreasing - rate of creep strain. This is the so called primary creep stage. After that the creep strain rate becomes nearly constant, this stage is known as secondary creep. If the creep process is not stopped there will be a third stage - the tertiary creep - which shows the opposite behaviour of primary creep and is immediately followed by the rupture of the structure.

In fact the total displacement in the experiment (black curve) shows a very different behaviour. The curve looks like a tertiary creep curve, but considering the stress and temperature regimes at this time and the total duration of 3 hours tertiary creep is very unlikely.

Performing a transient calculation with a changing temperature field according to the recorded power input (cf. Fig. 2) the calculated creep follows the red curve in Figure 10. For this calculation the steady state temperature fields of the CFD-calculations with 30, 35 and 40kW were considered and a time delay of 15min between the power change and the change of the temperature field was assumed. Consequently the temperature at the beginning of the creep deformation stage is decreasing due to a power decrease just before pressurization (cf. Fig. 2 and 3). From this relatively low level the temperature increases after the first half hour of creep until heater failure. Within these steps the temperature is linearly interpolated. Of course this model has to

be improved and as mentioned before this will be possible with a transient temperature field available from the CFD-result file.

Figure 11 shows the von Mises equivalent stress and the total displacement of the vessel at the time of heater failure. As mentioned the heater failure occurred due to the uncovering of the top ends of the heater rods. A volume calculation of the deformed vessel shows that the melt level at this time had dropped by 33mm, assuming a total height of the melt of 188mm at the beginning.

Comparing Figures 12 and 13 it can be seen that the calculation fits with the experimental data not at all geometrical positions. The discrepancies are greater in the upper part of the hemisphere and at the beginning of the cylindrical part. This could be due to the vertical offset of the calculated temperature field and the measured one. The effect of the offset is eliminated in the lower parts ($134^\circ < T < 180^\circ$) where the calculation is in good agreement with the experiment.

The most interesting question for the next experiment is the vessel failure time. It is not intended to have the vessel fail at the high pressure load. Therefore, different scenarios have to be calculated. In the calculations shown here the temperature increase after the unintentional heater failure in FOREVER-C2 has been set to 10K/h and the high pressure load was kept on until vessel failure. With an assumed very conservative creep rupture strain of $\epsilon^{\text{frac}}=20\%$ for all stresses and temperatures for the evaluation of the damage parameter D , leads to a vessel failure at $t_{\text{frac}}=23700\text{s}$. This means just 15min after the heater failure the vessel would have failed. But considering the uniaxial creep test data of the 16MND5-steel (Ikonen, 1999) and the results of the Lower Head Failure Tests (Chu et al., 1999) at the Sandia National Laboratories even a creep rupture strain of $\epsilon^{\text{frac}}=40\%$ can be stated as conservative. Figure 14 shows the total displacement at $T=134^\circ$ for both cases. In the 40%-scenario failure could be expected after $t_{\text{frac}}=28800\text{s}$, which means more than one hour after heater failure in FOREVER-C2. Of course, this is a first estimate and additional analysis will be performed.

SUMMARY AND OUTLOOK

In this paper a short description of the phenomena occurring in the course of the FOREVER experiments is given. The combined modelling strategy of thermo-fluid-dynamic and structure mechanical Finite-Element calculations is described and an advanced numerical creep and damage parameter model is presented.

The post test calculations of the FOREVER-C2 experiment show that the behaviour of the vessel - made of French RPV steel - is quite sensitive to temperature variations during the creep deformation stage. Therefore, it appears that the unexpected deformation behaviour during the experiment is caused by the transient temperature field in the vessel wall rather than by a tertiary creep process.

The model will be improved by employing the transient thermal boundary conditions which have a great influence on the transient creep calculation. First rupture estimations have shown that one of the main mechanical parameters to be investigated in the future is the failure strain.

ACKNOWLEDGEMENTS

The authors are grateful to Th. Moessner (Rossendorf) who supported the programming work for the customized ANSYS code. The FOREVER C1 experiment was performed under the partial sponsorship of EU. The FOREVER C2 experiment was performed under the sponsorship of the APRI Project of the SKI, Swedish and Finish Power Companies, USNRC, and HSK. This work was performed by the first author at RIT.

REFERENCES

- ANSYS, 1998, Programmer's Manual. ANSYS, Inc.
- Azodi, D., P. Eisert, U. Jendrich, W.M. Kuntze, 1996, GRS-Report GRS-A-2264.
- Becker, A.A., Background to Material Non-Linear Benchmarks. NAFEMS-report R0049 (International Association for the Engineering Analysis Community).
- Chu, T.Y., Pilch, M.M., Bentz, J.H., Ludwigsen, J.S., Lu, W.Y., Humphries, L.L., 1999, "Lower Head Failure Experiments and Analyses", Report, NUREG/CR-5582, SAND98-2047, Sandia National Laboratories, Albuquerque, NM, USA.
- Ikonen, K., 1999, "Creep Model Fitting Derived from REVISA Creep, Tensile and Relaxation Measurements", Technical Report MOSES-4/99, VTT-Energy, Espoo, Finland.
- James, A.M., Lord, M.P., 1992, "Macmillan's Chemical and Physical Data", The Macmillan Press, London, GB.
- Launder, B.E., Spalding, D.B., 1974, "The Numerical Computation of Turbulent Flows", Computer Methods in Applied Mechanics and Engineering 3, pp. 269-289.
- Sehgal, B.R., Nourgaliev, R.R., Dinh, T.N., Karbojian, A., 1999, "FOREVER experimental program on reactor pressure vessel creep behavior and core debris retention", Proceedings of the 15-th International Conference on Structural Mechanics in Reactor Technology (SMiRT-15), Seoul, Korea, August 15-20, 1999.
- Sehgal, B.R., Nourgaliev, R.R., Dinh, T.N., 1999, "Characterization of heat transfer processes in a melt pool convection and vessel-creep experiment", NURETH-9, San Francisco, Oct. 3-8, 1999.
- Sala, A., 1984, "Radiant Properties of Materials, Tables of Radiant Values for Black Body and Real Materials", Elsevier, Amsterdam.

Verein Deutscher Ingenieure, 1994, "VDI-Waermeatlas, Berechnungsblaetter für den Waermeuebergang", 7. Auflage, VDI-Verlag, Duesseldorf, Germany.

APPENDIX

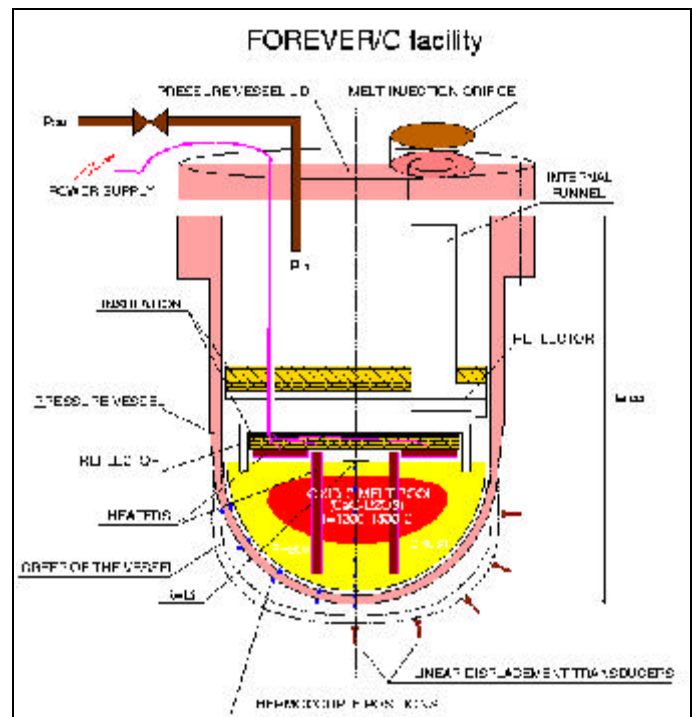


Fig. 1: Principal scheme of the FOREVER/Creep tests. Scheme is not to scale.

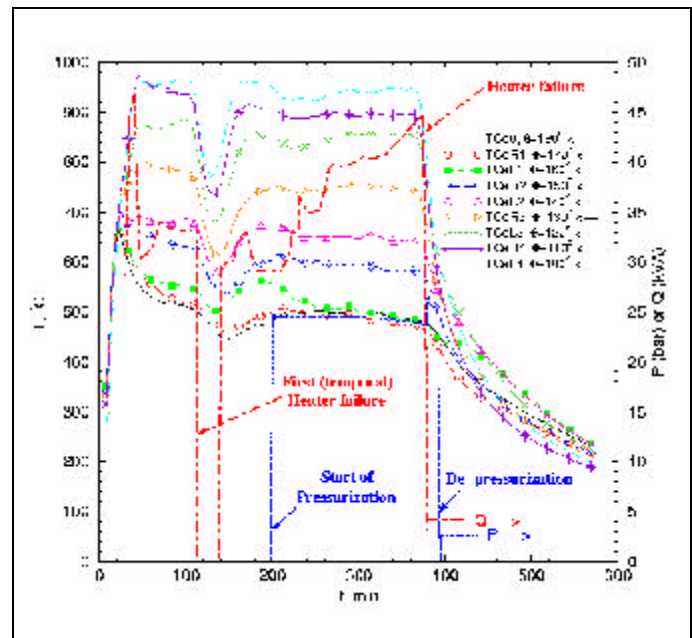


Fig. 2: General course of the experiment C2: power input Q / [kW], pressure P / [bar] and external temperatures T / [°C]. $\Theta = 180^\circ$ refers to the very bottom of the hemispherical bottom head.

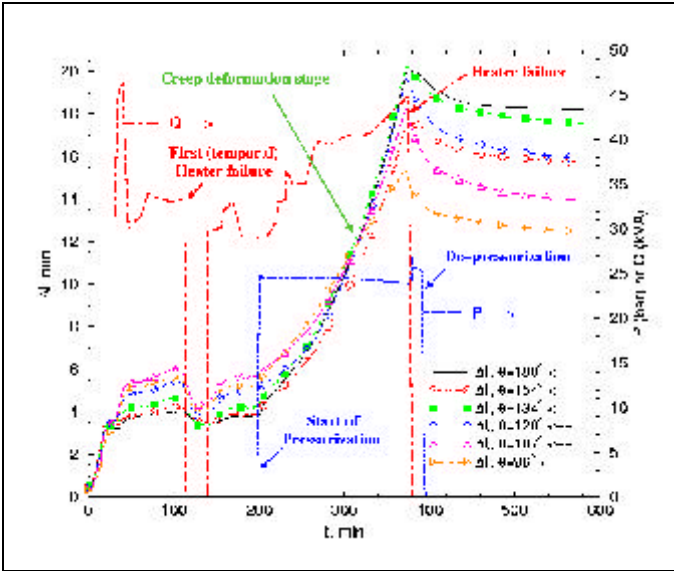


Fig. 3: General course of the experiment C2: power input Q / [kVA], pressure P / [bar] and total displacement U_{sum} / [mm] at different external positions of the hemisphere. $\Theta = 180^\circ$ refers to the very bottom of the hemispherical bottom head..

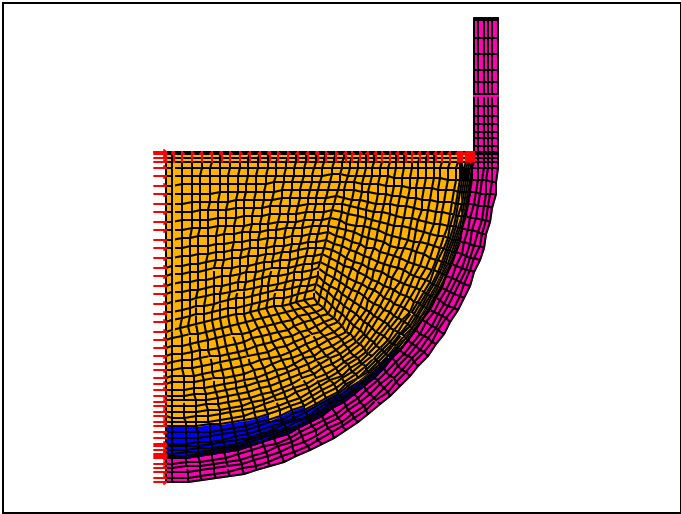


Fig. 5: Mesh, fluid-dynamic boundary conditions and material definition of the CFD-model after reaching quasi-stationary state with input power $Q=35\text{kW}$ and dynamic crust formation. Colours: magenta=solid steel, blue=solid oxidic crust, orange=liquid oxid. Cylindrical part is not fully shown.

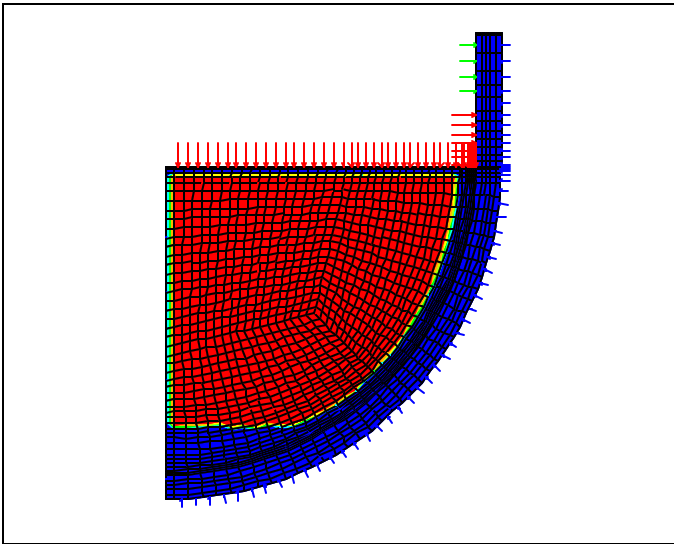


Fig. 4: Axis-symmetric 2D-thermo-fluid-dynamic FE-Model of the FOREVER-C2-experiment. Red coloured area indicates volumetric heat generation zone. Length and colour of arrows corresponds to the applied ambient temperature for radiative heat transfer boundary condition. Cylindrical part is not fully shown.

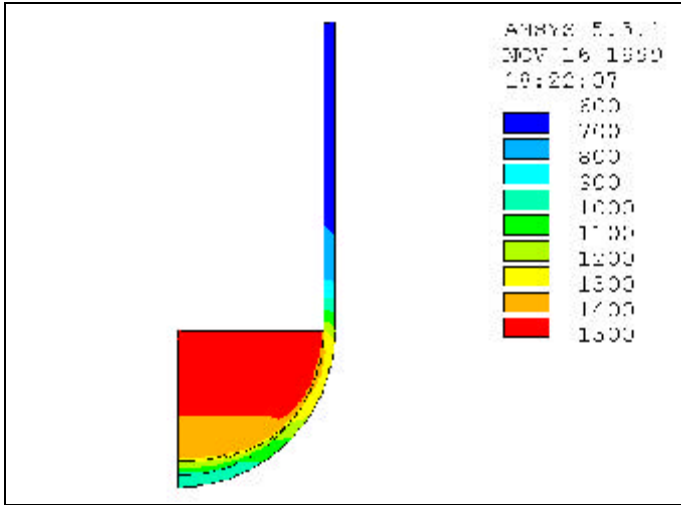


Fig. 6: Calculated temperature field within whole computational domain after reaching quasi-stationary state with a power input of $Q=35\text{kW}$. T in [K]. Model figure is to scale and shown completely.

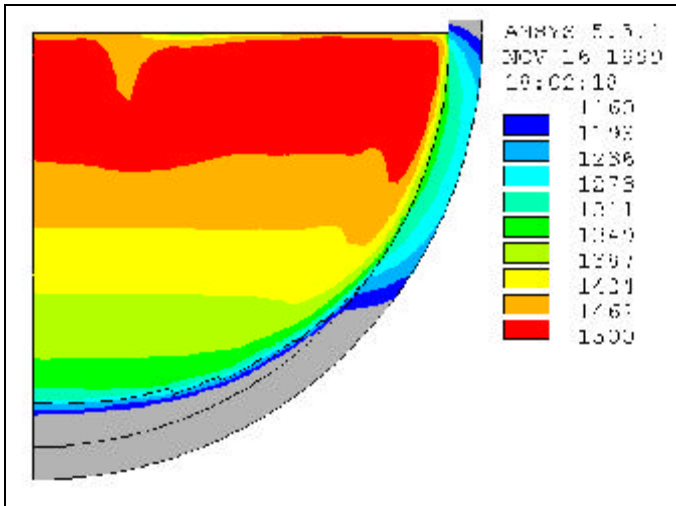


Fig. 7: Calculated temperature field in the hemispherical part with a power input of $Q=35\text{kW}$. T in [K], adjusted scale ranges from 1160K to 1500K, temperatures below 1160K are presented grey.

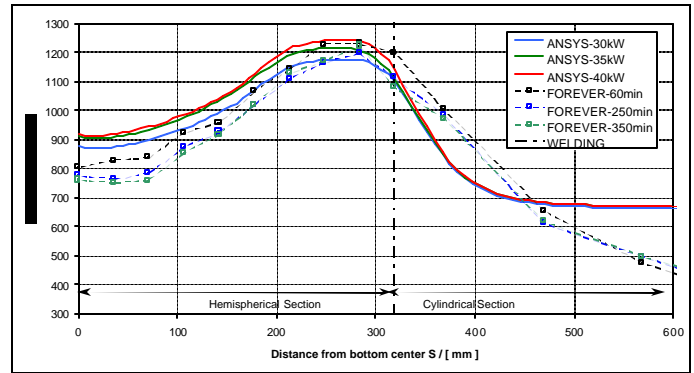


Fig. 8: Comparison of external vessel surface temperature T / [K] at different times during the experiment and that calculated by ANSYS for different power inputs. Abscissa starts at very bottom centre and shows the chord length to the top of the cylinder.

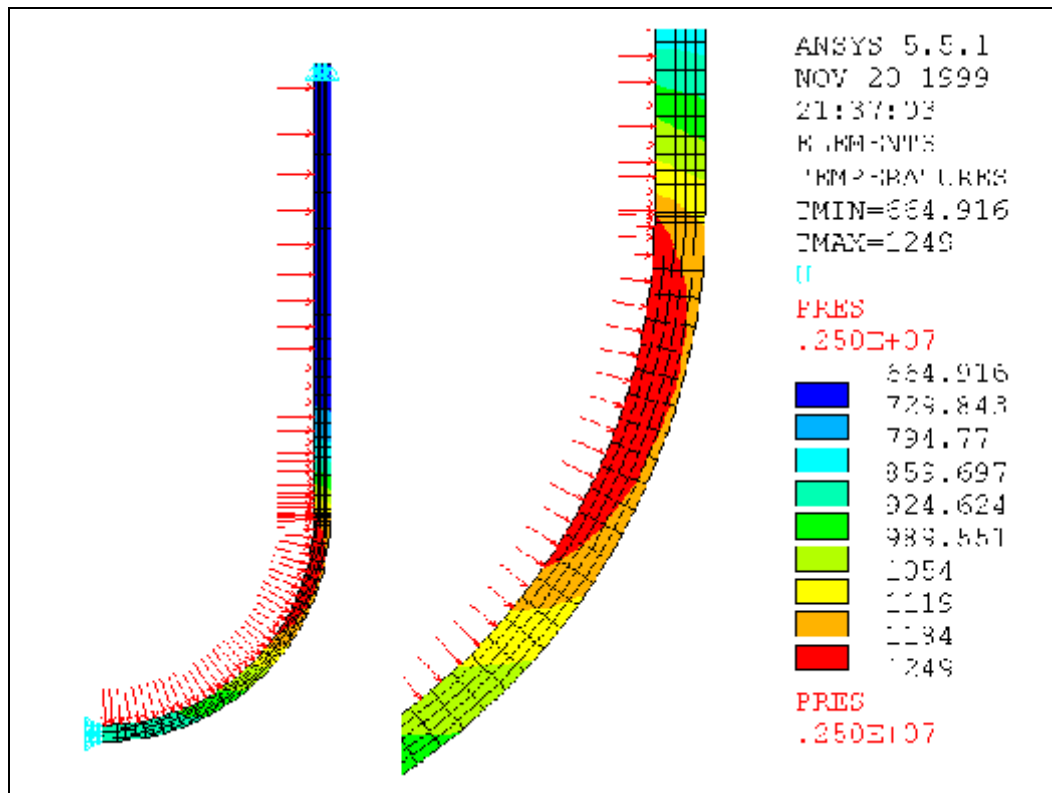


Fig. 9: Mechanical FE-model with applied boundary conditions, surface loads and body loads: $U_y=0$ at top, $U_x=0$ at symmetry line, internal pressure $P=2.5\text{MPa}$, temperature field caused by power input $Q=30\text{kW}$. Left side total view, right side detail of hot focus region.

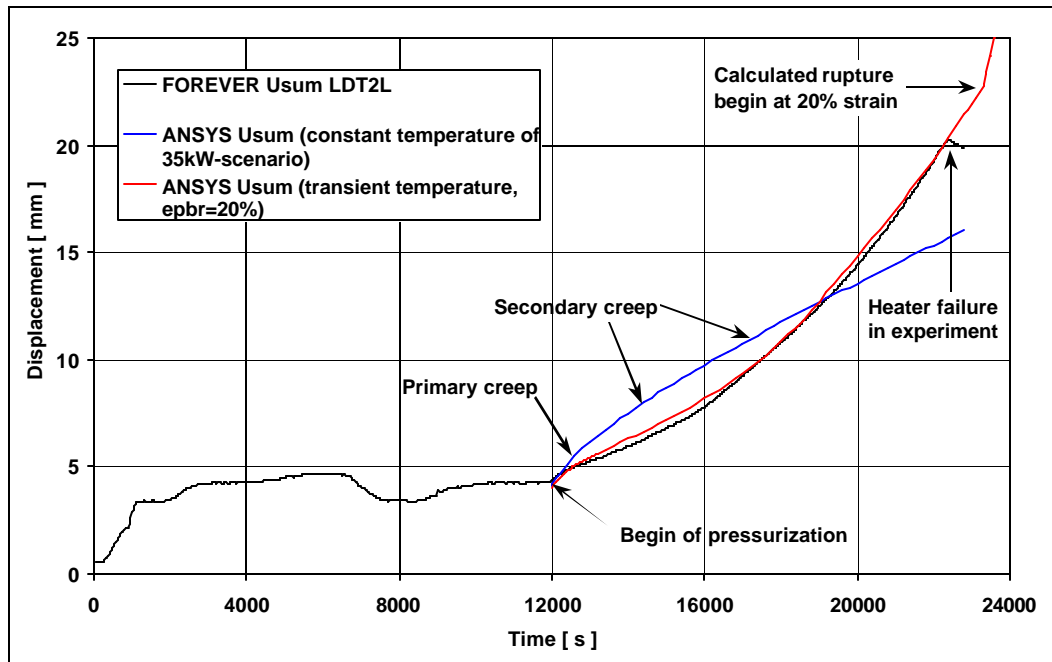


Fig. 10: Total displacement U_{sum} / [m] of the vessel external surface on the left side at position $\Theta = 134^\circ$ over time t / [s].

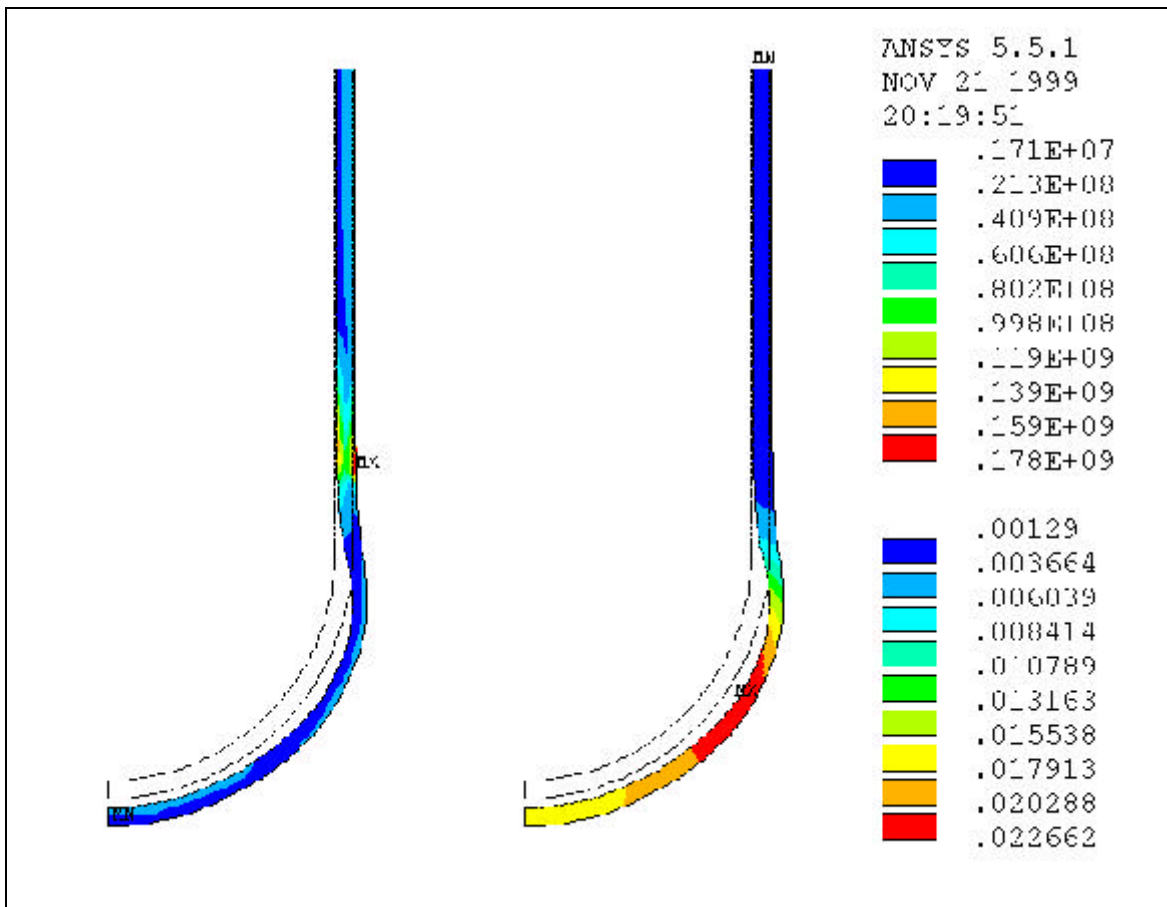


Fig. 11: Von Mises equivalent stress σ_{eqv} [Pa] (left side and upper scale and total displacement U_{sum} / [m] (right side and lower scale) of the vessel after $t=22800$ s (heater failure).

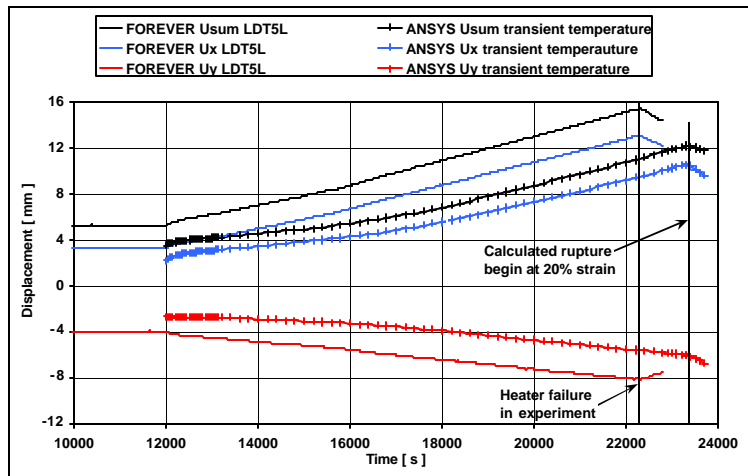


Fig. 12: Total displacement U_{sum} / [m], horizontal displacement U_x / [m] and vertical displacement U_y / [m] of the vessel external surface on the left side at position $\Theta = 96^\circ$ over time t / [s].

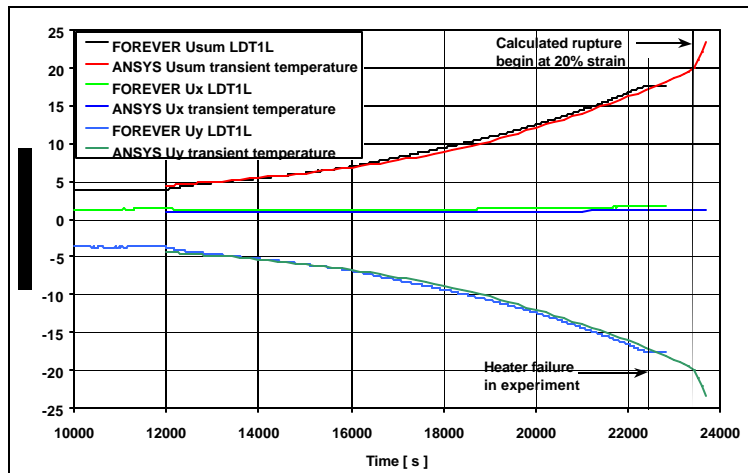


Fig. 13: Total displacement U_{sum} / [mm], horizontal displacement U_x / [mm] and vertical displacement U_y / [mm] of the vessel external surface on the left side at position $\Theta = 154^\circ$ over time t / [s].

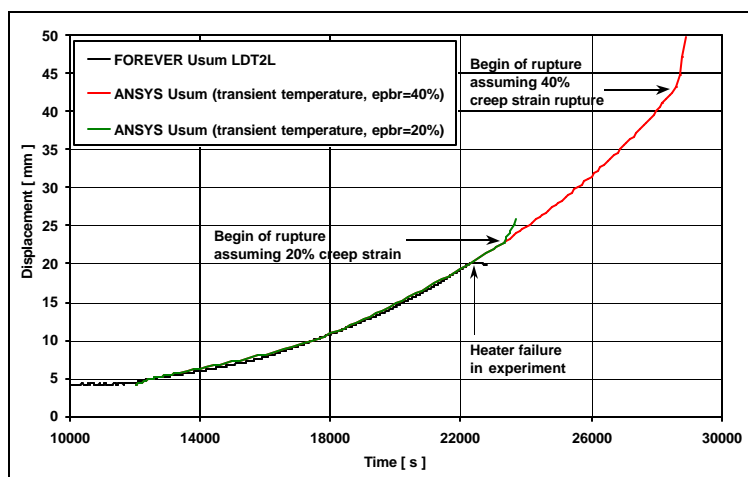


Fig. 14: Estimation of vessel failure time with different creep rupture strains. Total displacement U_{sum} / [mm] of the vessel external surface on the left side at position $\Theta = 134^\circ$ over time t / [s].